Transport in Porous Media (2005) 61: 337–363
DOI 10.1007/s11242-005-0261-4

Saltwater Upconing and Decay Beneath a Well Pumping Above an Interface Zone

QUANLIN ZHOU[1,*], JACOB BEAR[2] and JACOB BENSABAT[3]
[1]*Earth Sciences Division, Lawrence Berkeley National Laboratory, Berkeley, CA 94720, U.S.A.*
[2]*Faculty of Civil & Environmental Engineering, Technion-Israel Institute of Technology, Haifa, Israel*
[3]*Environmental and Water Resources Engineering Inc., PO Box 6770, Haifa 31067, Israel*

(Received: 16 February 2004; accepted in final form: 5 January 2005)

Abstract. Saltwater, or brine, underlies freshwater in many aquifers, with a transition zone separating them. Pumping freshwater by a well located above the transition zone produces upconing of the latter, eventually salinizing the pumped water, forcing shut-off. Following the well's shut-off, the upconed saltwater mound undergoes decay, tending to return to the pre-pumping regime. The FEAS code is used for the simulation of coupled density-dependent flow and salt transport involved in the upconing–decay process. In this code, the flow equation is solved by the Galerkin finite element method (FEM), while the advective–dispersive salt transport equation is solved in the Eulerian–Lagrangian framework. The code does not suffer from the instability constraint on the Peclet number. The code is used to investigate the transient upconing–decay process in an axially symmetric system and to discover how the process is affected by two major factors: the *density difference factor* (DDF) and the dispersivities. Simulation results show that under certain conditions, pumping essentially freshwater can be maintained for a certain time period, the length of which depends on the dispersivity values used. A recirculating flow cell may occur in the saltwater layer beneath the pumping well, widening the saltwater mound. The decay process is lengthy; it takes a long time for the upconed saltwater to migrate back to its original shape of a horizontal transition zone prior to pumping. However, the wider transition zone caused by hydrodynamic dispersion can never return to the initial one. This indicates that once a pumping well is abandoned because of high salinity, it can be reused for groundwater utilization only after a long time. It is also shown that the upconing–decay process is very sensitive to DDF, which, in our work, ranges from 0 (for an ideal tracer) to 0.2 (for brine). For a DDF of 0.025 (for seawater), local upconing occurs only for low iso-salinity surfaces, while those of high salt concentration remain stable after a short time. For an ideal tracer, all iso-salinity surfaces rise toward the pumping well, whereas for brine only iso-salinity surfaces of very low salinity upcone towards the pumping well. This may imply that the traditional finding that the sharp interface approximation is practically close to the 0.5 iso-salinity surface may not be true for a high DDF solution.

Key words: seawater intrusion, saltwater upcoming, brine, density-dependent flow, particle tracking

*Author for correspondence: Tel.: +1-510-486-5344; Fax: +1-510-486-5686; e-mail: qlzhou@lbl.gov

1. Introduction

Brine, or saltwater, underlies freshwater in many inland aquifers (e.g., Ma *et al*., 1997), with a *transition zone* separating them. The screened portions of pumping wells are often located within the freshwater zone that overlies the transition zone. We shall also use the term "interface zone" for this transition zone. During pumping, the transition zone *upcones* towards the screened portion of the well, and, the salinity of the pumped water gradually increases. When pumping is constrained below some "critical pumping rate", the well may pump essentially freshwater (say, keeping salinity less than 2% of saltwater). When the pumping rate is increased, the well will be salinized and the pumping will have to be shut-off. Following the shut-off, the upconed saline water mound decays, due mainly to gravity imbalance. The well may be restarted after the aquifer recovers from the influence of the previous pumping period. This pumping policy may increase the efficiency of freshwater pumping from the aquifer. This local upconing and decay processes can be superimposed on the regional seawater intrusion regime in a coastal aquifer (Bear *et al*., 2001).

Until recently, many sharp interface approximation models have been employed to investigate the problem of interface upconing, primarily in connection with seawater intrusion in coastal aquifers (e.g., Bear and Dagan, 1964; Bear, 1979; Dagan and Zeitoun, 1998). Up to a certain critical pumping rate, the sharp interface does not reach the well, and the latter continues to pump freshwater. At some critical pumping rate, the (assumed sharp) interface takes the shape of a very unstable cusp, and any increase in the pumping rate will immediately bring the interface, and with it saltwater, into the pumping well. Under such conditions, the assumption of a sharp interface is no longer valid, and models based on it cannot be used. Analytical, experimental, and numerical methods have been employed to determine the position of the sharp interface and the critical pumping rate. A number of exact and approximate analytical solutions have been obtained for local upconing in the case of steady flow in homogeneous aquifers (Muskat and Wyckoff, 1935; Muskat, 1937; Strack, 1972; Bower *et al*., 1999). Dagan and Zeitoun (1998) developed an analytical solution for interface upconing in a stratified aquifer with a random hydraulic conductivity. Hele–Shaw analogs (that model flow in a vertical plane) were employed to verify the approximate analytical solutions (Muskat, 1937; Bennett *et al*., 1968; Haubold, 1975). Numerical modeling has become a powerful tool for investigating upconing in field applications. Sahni (1973) developed a finite difference model for the simulation of the upconing problem. Pinder and Page (1977) obtained the local upconing under a pumping well by solving for the regional interface under an island. Reilly *et al*. (1987) applied a finite element model to estimate

the maximum steady-state permissible discharge rate in an inland groundwater system. Kemblowski (1987) investigated the impact of the Duipuit–Forchheimer approximation on the simulation of upconing. He found that this approximation might produce large errors in estimating the upconing beneath a point drain, but produces good results for that below a river, which is wide relative to the thickness of aquifer. Haitjema (1991) developed an analytic element model for an axi-symmetric transient interface flow, including density and viscosity differences between the two immiscible fluids. However, the sharp interface models neglect the effect of hydrodynamic dispersion on upconing, and they often overestimate the critical pumping rate.

The transition zone model for upconing takes into account hydrodynamic dispersion in the real world. Since in this model flow and salt transport are coupled by the fluid's variable density, only numerical techniques are available to solve the nonlinear and coupled flow and salt transport equations. Rubin and Pinder (1977) described upconing as a migration of a sharp interface perturbed by a small disturbance that results from dispersion. Wirojanagud and Charbeneau (1985) superposed the effect of hydrodynamic dispersion on a sharp interface solution. During the last two decades, a number of computer codes have been developed for simulating the coupled density-dependent flow and salt transport (Bear *et al.*, 1999). For example, Diersch *et al.* (1984) simulated a local upconing problem in cylindrical coordinate using the finite element code FEFLOW. Reilly and Goodman (1987) obtained solutions to a local upconing problem, using the SUTRA code. They compared their solutions with the sharp interface approximations obtained by Bennett *et al.* (1968), and found that the sharp interface model overestimates the critical pumping rate, although the 0.5 iso-concentration surface is close to the sharp interface configuration in the area away from the pumping well. Ma *et al.* (1997) applied the SWIFT-II code to an upconing problem of saltwater in a bedrock brine aquifer to the overlying alluvial aquifer. The success of these applications depends mainly on the magnitude of numerical dispersion. The numerical dispersion is associated with the numerical solution of the advective–dispersive salt transport equation using the finite element or finite difference method in the Eulerian framework used in these computer codes (Neuman, 1984; Bensabat *et al.*, 2000). Particularly, such numerical dispersion may be large in the advection-dominated flow field around the pumping well.

Most of the previous research on the upconing problem, using either the sharp interface model or the transition zone model, has paid much attention to determining the critical pumping rate for water supply in freshwater aquifers. Few simulations have been conducted to investigate the decay phenomenon that takes place after the shut-off of salinized wells. In addition, few applications have focused on the upconing problem for saltwater

of different density contrasts between pure saltwater and freshwater. Different density contrasts may produce very different upconing phenomena. For example, Oswald (1998) and Oswald *et al*. (2002) conducted a series of laboratory experiments on saltwater upconing using solutions with different salt concentrations in a three-dimensional cubical domain. The experimental results demonstrated that the saltwater upconing regime is very sensitive to the density contrast between the salt solution and freshwater.

The objective of the paper is to present (1) the detailed mechanisms of flow and salt transport involved in the upconing problem, (2) the decay phenomenon after the shut-off of a salinized well, and (3) the effects of different density contrasts between freshwater and saltwater and of the magnitude of transport parameters (dispersivity). The sensitivity of density contrasts significantly improves our understanding of flow and salt transport phenomena in the upconing–decay process. In Section 2, we start by presenting the coupled density-dependent flow and salt transport model, solved by the computer code FEAS. A brief description of the numerical schemes employed in FEAS is presented in Section 3. The application to the transient upconing–decay process beneath a pumping well in an axially symmetrical system is presented in Section 4, with a detailed discussion of transport phenomena.

2. Mathematical Model

The general mass balance equations for an aqueous liquid phase and for a dissolved solute component (salt) provide the governing equations for the strongly coupled density-dependent flow and salt transport (Bear and Verruijt, 1990; Bear and Bachmat, 1991). It is assumed that the generalized Darcy's law and a Fickian-type law are valid for the fluid's motion and for the dispersive flux, respectively. We do not include the cross-coupling terms in Darcy's law and dispersive flux for high concentration of brine, as suggested by Hassanizadeh and Leijnse (1988).

2.1. CONSTITUTIVE EQUATIONS

Because in this work, we consider two fluid layers: a layer of low salt concentration (to which we refer as "freshwater") and a layer of high salt concentration (seawater or brine, to which we refer as "saltwater"), it is convenient to introduce a *normalized mass fraction* of salt in solution, $C\,(=(\omega-\omega_{\mathrm{fw}})/(\omega_{\mathrm{sw}}-\omega_{\mathrm{fw}}))$, for the mixed water in the transition zone between the freshwater and saltwater layers. Note that ω is the mass fraction of salt (mass of dissolved salt per unit mass of fluid) of the aqueous liquid phase, and ω_{fw} and ω_{sw} are the salt mass fractions of freshwater and of saltwater, respectively.

A simplified relationship between fluid density, ρ, and the normalized mass fraction of salt is typically written as

$$\rho = \rho_{\mathrm{fw}}\,(1 + \beta_C C)\,, \tag{1}$$

where ρ_{fw} is the freshwater density, and β_C is a *density difference factor* (DDF). It is assumed that for the range of pressures considered here, the pressure effect on fluid density is negligible in comparison with the salt concentration effect.

The fluid's dynamic viscosity, μ, varies with the salt mass fraction, ω, in the form:

$$\mu = \mu_{\mathrm{fw}}\mu_r = \mu_{\mathrm{fw}}\left(1 + 1.85\omega - 4.1\omega^2 + 44.50\omega^3\right), \tag{2}$$

which is based on experimental data from Weast (1989), with fitting by Lever and Jackson (1985) and Hassanizadeh and Leijnse (1988). The symbol μ_{fw} represents the freshwater dynamic viscosity, and μ_r is the relative viscosity.

2.2. DENSITY-DEPENDENT FLOW EQUATION

The general mass balance equation for the aqueous phase takes the form (Bear and Bachmat, 1991)

$$\frac{\partial \phi \rho}{\partial t} = -\frac{\partial \rho q_i}{\partial x_i} + (\rho^* Q_R - \rho Q_P) \tag{3}$$

with the injection and pumping through wells represented, symbolically, by

$$\rho^* Q_R = \sum_n \rho_n^* Q_{Rn}(\mathbf{x}_n, t)\delta(\mathbf{x} - \mathbf{x}_n),$$
$$\rho Q_P = \sum_m \rho_m Q_{Pm}(\mathbf{x}_m, t)\delta(\mathbf{x} - \mathbf{x}_m),$$

where x_i ($i = 1, 2, 3$ in three dimensions) is the ith component of the position vector, $\mathbf{x}$, in the Cartesian coordinates, t is the time, ϕ is the porosity, q_i is the ith component of the specific discharge vector $\mathbf{q}$, Q_{Rn} and ρ_n^* are the injection rate, and fluid's density of water injected through a well at point $\mathbf{x}_n$, respectively, Q_{Pm} and ρ_m are the pumping rate and density of water pumped through a well at point $\mathbf{x}_m$. For the sake of simplicity, we shall, henceforth, refer to the aqueous liquid phase as salt solution or as "water".

We may rewrite Equation (3) in the form (Bear and Verruijt, 1990):

$$\rho S_{0p}\frac{\partial p}{\partial t} + \rho\phi\beta_C\frac{\partial C}{\partial t} = -\frac{\partial \rho q_i}{\partial x_i} + (\rho^* Q_R - \rho Q_P), \tag{4}$$

where $S_{0p}\left(=\phi\beta_p+\alpha\right)$ is the specific storativity with respect to pressure changes, β_p is the coefficient of compressibility of the fluid, $\alpha\,(=-(1/(1-\phi))d(1-\phi)/dp)$ denotes the coefficient of solid matrix compressibility (with $\alpha=0$ for the nondeformable material considered here), and p is the fluid's pressure.

The generalized Darcy's law for a variable density fluid takes the form:

$$q_i \equiv \phi V_i = -\frac{k_{ij}}{\mu}\left(\frac{\partial p}{\partial x_j}+\rho g\frac{\partial x_3}{\partial x_j}\right), \tag{5}$$

where V_i is the ith component of the velocity vector, k_{ij} is the permeability tensor, g is the gravitational acceleration, and x_3 is the vertical component of the Cartesian coordinates. After the introduction of a reference freshwater head, $h_f = h_f(x_1, x_2, x_3, t)$, as a primary variable:

$$h_f = \frac{p}{\rho_{\mathrm{fw}} g}+x_3. \tag{6}$$

Darcy's law can be rewritten as:

$$q_i = -\frac{K_{ij}^f}{\mu_r}\left(\frac{\partial h_f}{\partial x_j}+\beta_C C\frac{\partial x_3}{\partial x_j}\right), \tag{7}$$

where $K_{ij}^f\left(=\rho_{\mathrm{fw}} g k_{ij}/\mu_{\mathrm{fw}}\right)$ is the reference hydraulic conductivity, related to the reference density ρ_{fw} and to the reference dynamic viscosity μ_{fw}.

By inserting Equations (6) and (7) into the mass balance equation, Equation (4), we obtain the density-dependent flow equation:

$$S_0\frac{\partial h_f}{\partial t}+\frac{\rho\phi\beta_C}{\rho_{\mathrm{fw}}}\frac{\partial C}{\partial t}=\frac{\partial}{\partial x_i}\left(K_{ij}\left(\frac{\partial h_f}{\partial x_j}+\beta_C C\frac{\partial x_3}{\partial x_j}\right)\right)+\frac{(\rho^* Q_R-\rho Q_P)}{\rho_{\mathrm{fw}}}, \tag{8}$$

where $K_{ij}\left(=\rho g k_{ij}/\mu\right)$ is the hydraulic conductivity, and $S_0\left(=\rho g\left(\phi\beta_p+\alpha\right)\right)$ is the specific storativity. Note that K_{ij} and S_0 vary in both space and time, depending on the mass fraction of the salt solution.

2.3. SALT TRANSPORT EQUATION

The mass balance for the dissolved matter (salt) can be expressed, in terms of the normalized mass fraction, in the form (Bear and Verruijt, 1990):

$$\frac{\partial\phi\rho C}{\partial t}=-\frac{\partial}{\partial x_i}\left(\rho C q_i-\phi\rho D_{ij}\frac{\partial C}{\partial x_j}\right)+\left(\rho^* C^* Q_R-\rho C Q_P\right) \tag{9}$$

with the injection and pumping through wells represented, symbolically, by

$$\rho^* C^* Q_R = \sum_n \rho_n^* C_n^* Q_{Rn}(\mathrm{x}_n, t)\delta(\mathrm{x} - \mathrm{x}_n),$$
$$\rho C Q_P = \sum_m \rho_m C_m Q_{Pm}(\mathrm{x}_m, t)\delta(\mathrm{x} - \mathrm{x}_m),$$

where C_n^* is the normalized mass fraction in the water injected through a well at point $\mathbf{x}_n$, $C_m(\equiv C(\mathbf{x}_m, t))$ is the normalized mass fraction in the water pumped through a well at point $\mathbf{x}_m$, and D_{ij} is the coefficient of hydrodynamic dispersion.

Expanding the first-order derivatives in Equation (9), and making use of the mass balance equation for water, Equation (3), we obtain

$$\phi\rho \frac{DC}{Dt} \equiv \phi\rho \left(\frac{\partial C}{\partial t} + V_i \frac{\partial C}{\partial x_i} \right) = \frac{\partial}{\partial x_i} \left(\phi\rho D_{ij} \frac{\partial C}{\partial x_j} \right) + \rho^* Q_R \left(C^* - C \right), \quad (10)$$

where DC/Dt denotes the material derivative of C.

The density-dependent flow equation is coupled with the transport one by the two terms: $\frac{\partial}{\partial x_i}\left(K_{ij}\beta_C C \frac{\partial x_3}{\partial x_j}\right)$ (body-force term) and $\phi\beta_C \frac{\rho}{\rho_{\mathrm{fw}}} \frac{\partial C}{\partial t}$, in addition to the coupling effect of the density variation on K_{ij} and S_0. The transport equation is coupled with the flow equation by the velocity, which appears as part of the coefficient of hydrodynamic dispersion, and in the advective transport term. The two governing equations, Equations (8) and (10), are, thus, nonlinear and coupled; they must be solved simultaneously.

The coefficient of hydrodynamic dispersion, D_{ij}, is the sum of the coefficient of mechanical dispersion and the coefficient of molecular diffusion, D_{mij}^*, in an anisotropic porous medium (Bear, 1979; Bear and Verruijt, 1990):

$$D_{ij} = a_{ijkm} \frac{V_k V_m}{V} + D_{mij}^*, \qquad D_{mij}^* (= D_m T_{ij}^*), \quad (11)$$

in which D_m is the coefficient of molecular diffusion in a liquid, the second rank tensor $\mathbf{T}^*$ denotes the tortuosity of the porous medium, a_{ijkm} is a typical component of the (fourth rank) dispersivity tensor, V is the magnitude of the (average) velocity vector, $\mathbf{V}$, and $\boldsymbol{\delta}_{ij}$ denotes the *Kronecker delta*. For an *isotropic porous medium*, we have

$$D_{ij} = a_T V \delta_{ij} + (a_L - a_T) \frac{V_i V_j}{V} + D_m^* \boldsymbol{\delta}_{ij}, \quad (12)$$

where a_L and a_T are the longitudinal and transversal dispersivities, respectively.

3. Numerical Model

The mathematical flow model is solved by the Galerkin finite element method (FEM). Linear and bilinear basis functions are employed for a triangular mesh and for a quadrilateral mesh in two-dimensions, respectively. As a special case of the two dimensions, the two-dimensional radial coordinate system is also implemented. In three-dimensions, linear and bilinear basis functions are used for a tetrahedral and for a vertical triangular prism meshes. The FEAS code was developed for the simulation of brine transport in two- and three-dimensional groundwater systems, by solving the coupled density-dependent flow and salt transport equations. This code has been verified in a number of benchmark cases for coupled and decoupled flow and transport simulations (Zhou, 1999; Bensabat *et al*., 2000).

When solving the flow model, spurious velocity results from the inconsistency between the approximation of vertical gradient of reference head and fluid density (Voss and Souza, 1987; Herbert *et al*., 1988; Zhou *et al*., 2001) in the multi-linear approximation (see Equation (7)). To avoid this spurious velocity in the vertical direction, in the FEM formulation of Darcy's law, the FEAS code uses an element-averaged fluid density for the body-force term. Thus, a linear or a multi-linear basis function can be used for both the reference head and the mass fraction.

The advective–dispersive salt transport equation is solved in the Eulerian–Lagrangian framework. The Lagrangian mass fraction is derived by the adaptive pathline-based particle-tracking algorithm presented by Bensabat *et al*. (2000). The Galerkin FEM is then used to solve the remaining dispersion equation. In the particle-tracking algorithm, the tracking process is split along element boundaries on an inter-element basis. The sub-process within an element may be further refined along the particle's path by subdividing the travel time within this element into a number of travel-time increments. Whether this in-element pathline-based refinement is needed or not depends on the complexity of the local velocity field. Tracking errors are controlled by practical criteria related to the rate of variation in the particle's velocity (in magnitude and direction). A bilinear spatial and temporal interpolation of particle velocity is used to avoid the error introduced by the stepwise temporal approximation used in most existing models. The efficiency of the particle tracking is improved by adapting the tracking time in each tracking step. This adaptation is based on two particle-velocity indices and on their corresponding given criteria. The tracking process in regions where the velocity varies significantly is split into more tracking steps than in regions with smooth velocity variations. This adaptive particle-tracking algorithm performs very well in a complex flow field in a density-dependent flow and transport problem.

Thus, at each time step, there is a need to solve a set of nonlinear equations. Time integration is performed using a first-order approximation and an under-relaxation strategy, which tends to reduce the rate of convergence, but ensures a smoother, nonoscillating path to the solution. The linearization of the system is performed using the Picard method. At each Picard iteration, the resulting set of linear equations is solved by applying a robust *Incomplete Choleski Conjugate Gradient algorithm* (Ajiz and Jennings, 1984; Axelsson and Barker, 1984; Barrett *et al.*, 1994). Time step size is determined in an adaptive way, depending on the convergence rate.

4. Upconing and Decay Processes

4.1. MODEL DEVELOPMENT

We consider a problem of axially symmetrical upconing in a homogeneous, anisotropic confined aquifer, with unsteady pumpage from a partially penetrating well (see Figure 1). The 20 m long well screen is centered 10 m below the aquifer top. The well pumps water at a rate of 100 m^3/h. The well is shut-off when the normalized mass fraction of salt in the pumped water reaches the value of 2%. Recharge of water occurs along the external radial boundary located at $r = 2000$ m, where we assume that the effect of pumping is (practically) negligible. Along this radial boundary, a hydrostatic pressure distribution is assumed to be maintained, with the pressure (or the reference head) depending on the transient saline–water-density distribution. Initially, the aquifer contains freshwater in the upper portion ($22 \leqslant x_3 \leqslant 120$ m) and saltwater (= seawater or brine) in the lower one ($x_3 \leqslant 20$ m), with a 2 m thick transition zone. We have assumed that the thickness of the initial saltwater portion of the aquifer (20 m) is such that (practically) it does not affect the resulting upconing. This problem is a modification of the upconing problem presented by Reilly and Goodman (1987) and Voss and Souza (1987). In their model, a 16 m thick initial transition zone and fixed saltwater–mass-fraction distribution on the external radial boundary were specified, because they focused on the steady-state solution of the upconing problem. Here, we use a very thin transition zone at the initial time, and solution-dependent flow condition at the external radial boundary. We focus on the transient upconing–decay process and the period of pumping essentially freshwater. In addition, we allow for the influx of water and salt from the external radial boundary, while their model allows influx also from the bottom boundary, by maintaining a constant pressure condition on it.

To complete the mathematical model, we need boundary and initial conditions, as well as model parameters. The top and bottom boundaries are impervious to both flow and transport, because the aquifer is confined.

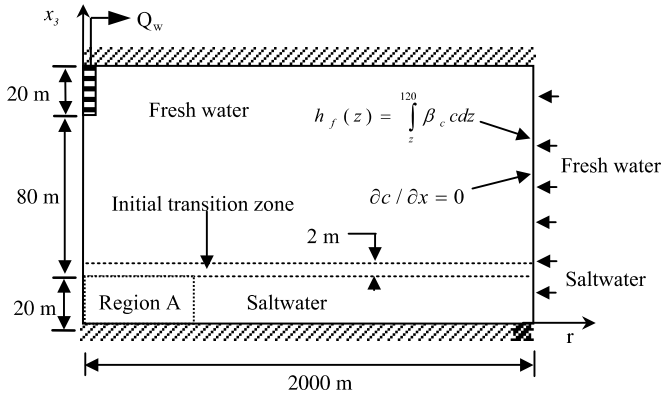

Figure 1. Initial and boundary conditions for the upconing problem in an axially symmetrical system.

The inner radial boundary at $r = 0$ m (except the screened portion) is also a no-flow boundary for both flow and transport. On the external radial boundary, we assume that we are sufficiently far away from the well so that the flow is always (essentially) horizontal, and, hence, the pressure (or reference head) distribution is always hydrostatic. This head distribution is updated with time based on the solution for the mass-fraction distribution in each time step. For the salt transport, we assume that along this boundary, the iso-mass-fraction surfaces remain always horizontal (as they are initially). This means that a zero mass-fraction gradient is maintained normal to this radial boundary, and salt is brought into the system only by advection.

The aquifer medium and transport parameters are listed in Table I. Three different groups of dispersivities are chosen to investigate the effect of hydrodynamic dispersion on the flow and transport regimes. Molecular diffusion is assumed negligible under the investigated field conditions, so that a narrow transition zone can be maintained in a region far away from the pumping well. The small dispersivities in case B are chosen to show whether the FEAS code can produce a narrow transition zone with small or no *numerical dispersion*. The density difference factor in the basic case is $\beta_C = 0.025$, which is a common value for seawater.

To investigate the effect of the density difference factor, β_C, on the upconing–decay process, we also simulate the transient flow and transport under different β_C values, ranging from 0.0 (for an ideal tracer) to 0.2 (for brine), with $\alpha_L = 1.0$ m and $\alpha_T = 0.5$ m.

Figure 2 shows a finite element mesh for an axially symmetrical problem. The mesh consists of 113×60 nonuniform rectangular finite elements and 114×61 nodes. The horizontal discretization increases from a spacing of 0.5 m close to the inner radial axis to a constant spacing of 25 m for $r \geqslant 50$ m. Uniform discretization of 2 m is used for the vertical direction.

Table I. Model parameters for the upconing problem

Parameter		Value
Porosity		$\phi = 0.2$
Horizontal permeability		$k_x = 2.56 \times 10^{-11}\ \mathrm{m}^2$
Vertical permeability		$k_z = 1.0 \times 10^{-11}\ \mathrm{m}^2$
Dynamic viscosity		$\mu = 1.0 \times 10^{-3}\ \mathrm{kg/ms}$
Gravity acceleration		$g = 9.81\ \mathrm{m/s}^2$
Pumping rate		$Q_w = 2400\ \mathrm{m}^3/\mathrm{d}$
Density of pure freshwater		$\rho_{fw} = 1000\ \mathrm{kg/m}^3$
Case A	Longitudinal dispersivity	$\alpha_L = 1\ \mathrm{m}$
	Transversal dispersivity	$\alpha_T = 0.5\ \mathrm{m}$
	Molecular diffusion coefficient	$D_m = 0\ \mathrm{m}^2/\mathrm{s}$
Case B	Longitudinal dispersivity	$\alpha_L = 0.2\ \mathrm{m}$
	Transversal dispersivity	$\alpha_T = 0.02\ \mathrm{m}$
	Molecular diffusion coefficient	$D_m = 0\ \mathrm{m}^2/\mathrm{s}$
Case C	Longitudinal dispersivity	$\alpha_L = 10\ \mathrm{m}$
	Transversal dispersivity	$\alpha_T = 1\ \mathrm{m}$
	Molecular diffusion coefficient	$D_m = 0\ \mathrm{m}^2/\mathrm{s}$

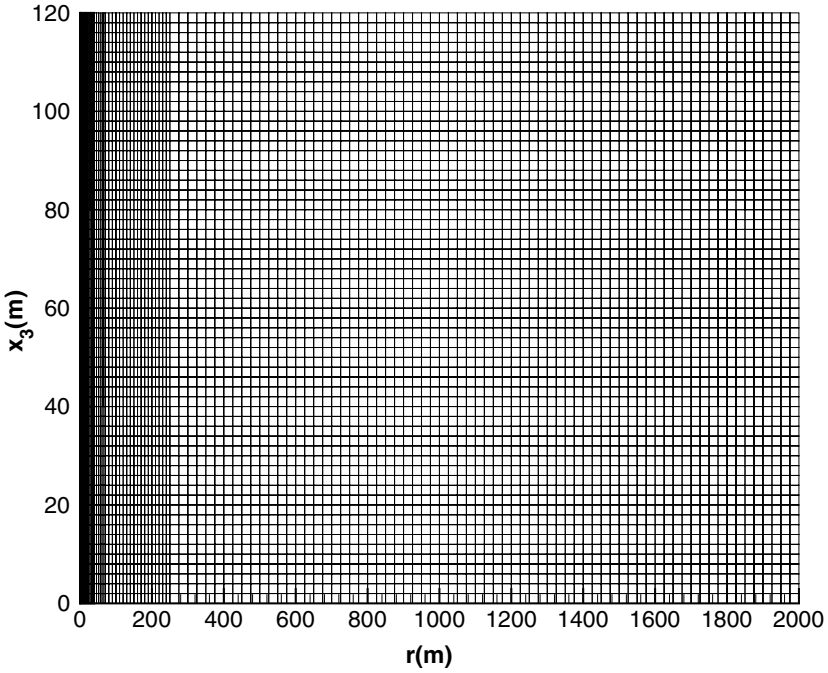

Figure 2. Finite element mesh for the upconing problem (113×60 rectangular elements).

We simulate the coupled flow and salt transport problem for each of the combinations of the set of transport parameters and the DDF. In each case, we simulate the transient upconing process until the well is shut off (when the normalized mass fraction in the pumped water reaches 2%), and the decay process, following the well's shut-off. For each case, the total simulation time is 50 years (the total simulation time is 80 years for brine case), and the time step size increases from the initial 0.01 to 50 days. The time step size is also cut back to 0.01 day immediately following the well's shut-off to accurately simulate the decay process.

4.2. RESULTS AND DISCUSSION

For the basic case with the dispersivities of $\alpha_L = 1.0\,\text{m}$, $\alpha_T = 0.5\,\text{m}$, and $\beta_C = 0.025$, we obtain the entire transient distributions of reference head, velocity, and normalized mass fraction in the 50 year period, which consists of the upconing period under pumping and decay period following the well's shut-off.

Initially, before pumping, we have a hydrostatic regime in the considered system. Both the normalized mass fraction and the reference head are constant in the horizontal direction. We have $C = 1$ for the saltwater zone at $0 \leqslant x_3 \leqslant 20\,\text{m}$ and $C = 0$ for the freshwater zone at $22 \leqslant x_3 \leqslant 120\,\text{m}$. Within the 2 m thick transition zone, the normalized mass fraction distribution varies linearly from $C = 1$ at its bottom to $C = 0$ at its top, because bilinear basis functions are used in the finite element model. The reference head is determined, based on the normalized mass fraction distribution. The head is selected as 10 m for the freshwater zone, and it is 10.525 m ($= 0.025 \times (0.5 \times 2\,\text{m} + 1.0 \times 20\,\text{m})$ at the bottom boundary caused by the density effect. Once pumping starts, a low reference head zone immediately occurs at the well screen. At the same time, the head beneath the pumping well also decreases, even in the transition zone and in the saltwater zone (see Figure 3a). Thus, the pumping induces saltwater inflow at the external radial boundary in both the saltwater and transition zones.

As pumping proceeds, salt is transported towards the well by advection and dispersion in the shape of a saltwater mound. As the upconing proceeds, the saltwater mound becomes higher in the vertical direction and wider in the horizontal direction. The simultaneous change in the normalized mass fraction has an effect on the reference-head distribution, because the flow is density-dependent (or mass-fraction-dependent) and coupled with transport. The flow field undergoes a number of changes.

First, the reference head at a point within the saltwater mound increases because of the cumulative effect of the fluid's density above it. The head increase depends on the thickness of the transition zone above the point, and on the normalized mass fraction distribution within the considered

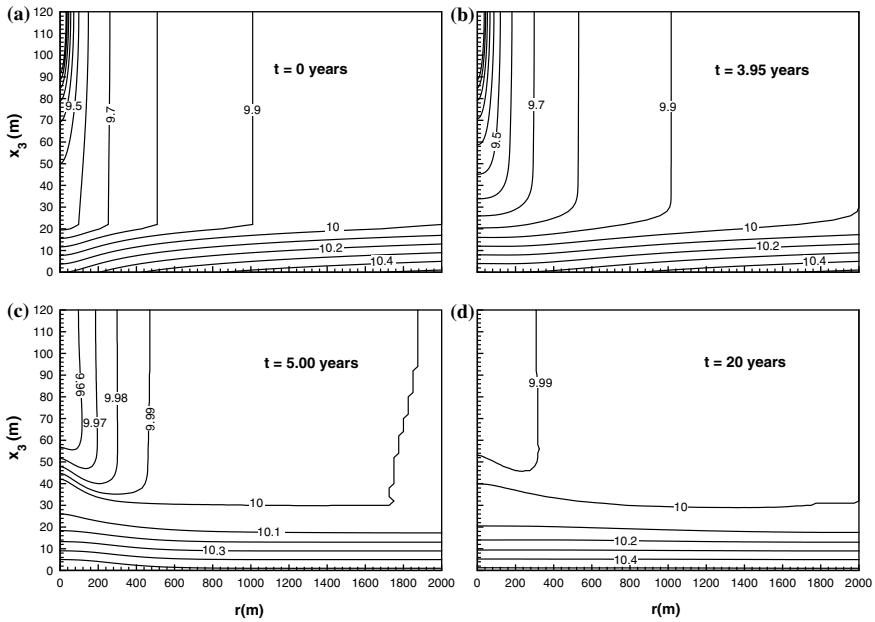

Figure 3. Reference head distributions at (a) initial time with pumping, (b) 3.95 years before well's shut-off, (c) 5 years, and (d) 20 years in the decay period in Case A with $\alpha_L = 1.0$ m and $\alpha_T = 0.5$ m and $\beta_c = 0.025$.

portion of the transition zone. Within the transition zone, the reference head is not distributed hydrostatically at early times, because there is a small vertical flow through this point. However, as upconing proceeds, the thickness of the transition zone beneath the pumping well increases, and the cumulative effect of the fluid's density at the point also increases (Figure 4). In the horizontal direction, a smaller fraction of the total saltwater inflow from the external radial boundary goes through the considered point, resulting in a smaller vertical flow at this point. To clearly demonstrate the transient processes of flow and transport in the vicinity of the well within the saltwater mound, we show, in Figure 4, the simulated reference head and normalized mass fraction along two vertical lines ($r = 20{,}100$ m) and two simulation times ($t = 0.5$, 3 years). At $t = 0.5$ years, we can see the head difference between the two vertical lines, although the difference is small in the lower portion of the transition zone. This difference decreases to essentially zero in the lower transition zone at $t =$ 3 years, resulting in no or very small horizontal flow. The reference head in the upper portion of the two vertical lines decreases with time, because the pumping rate and the reference head within the freshwater zone at the external radial boundary remain unchanged. This indicates that less

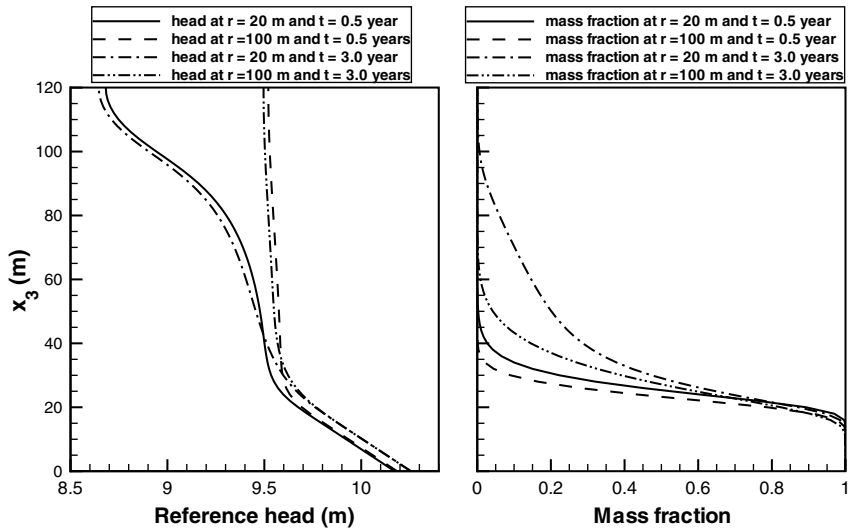

Figure 4. Vertical distributions of the simulated reference head and normalized mass fraction at $r = 20\,\text{m}$ and $100\,\text{m}$ and at $t = 0.5\,\text{years}$ and $t = 3\,\text{years}$ in case A.

horizontal flow in the lower transition zone results in more horizontal flow to the pumping well occurring in the upper freshwater zone.

Within the transition zone, particularly in its lower portion, the pressure distribution gradually approaches the hydrostatic one along the vertical (Figure 5). The reference head distribution (based on the assumed hydrostatic pressure distribution) at a point located within the lower transition zone, as a function of the x_3 coordinate, along the vertical line of r can be calculated by definition:

$$h_f^S(r, x_3) = h_f^*(r, 0) - \int_0^{x_3} \beta_C C(r, \xi) \mathrm{d}\xi, \tag{13}$$

where h_f^* is the simulated reference head at the point on the bottom boundary, $h_f^S(r, x_3)$ is the hydrostatic reference head, and $C(r, \xi)$ is the simulated normalized mass fraction. In Figure 5, we can see that the simulated and the assumed hydrostatic reference head distributions are close to each other in the lower portion of the transition zone (say, in the region of normalized mass fraction greater than 0.2 and less than 1.0). As the upconing proceeds, the hydrostatic zone expands in the vertical direction. For example, the quasi-hydrostatic zone is between 0 m and 30 m at $t = 0.5$ year, while it is between 0 m and 40 m at $t = 3$ years along the vertical line of $r = 20\,\text{m}$. Note that the saltwater zone beneath the saltwater mound quickly approach the hydrostatic (or quasi-hydrostatic) status (Figures 4 and 5).

As upconing continues, the velocity in both the vertical and horizontal directions decreases in the lower left corner region (defined as [0,

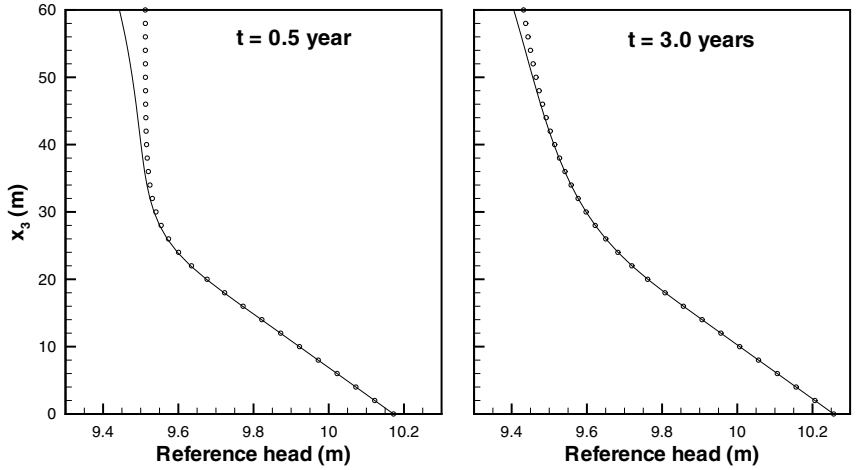

Figure 5. Vertical distributions of the simulated reference head (by solid lines) and the calculated head (by symbols) using hydrostatic status assumption at two different times at $r = 20$ m in case A.

200 m] $\times$ [0, 22 m] and shown as Region A in Figure 1). After 1.2 years, a stagnant, or a small recirculating, flow cell gradually develops as a result of the increase in the reference head beneath the well. Figure 6 demonstrates the process of the development of the recirculating flow regime. A separation of flow occurs at $x_3 = 24$ m along the inner radial boundary. The recirculating flow regime beneath the pumping well prevents saline water of high mass fraction in the lower portion of transition zone from migrating upward to the well. The increase in salt mass in the upper portion of the transition zone, especially in the saltwater mound, has to be supplied from a region farther away from the inner radial axis, widening the saltwater mound in the horizontal direction.

Coupled with the flow regime discussed above, the salt transport exhibits two different regimes in (a) the upconing region, say $0 \leqslant r \leqslant 800$ m, and (b) the far region away from the upconing region ($r > 800$) (see Figure 7). In the far region, the transition zone widens with time in the vertical direction because of the transversal hydrodynamic dispersion, which depends on the essentially horizontal flow in this region. Along the r-direction, the transition zone becomes narrower because velocity decreases in the axially symmetrical system. On the external radial boundary at $r = 2000$ m, the transition zone also widens with time because the boundary conditions used for flow and transport allow for the updating of mass fraction and reference head.

In the upconing region, two subregions of different transport features exist: the lower portion and the upper portion of the saltwater mound. For the lower portion, the mass fraction is relatively high and the flow

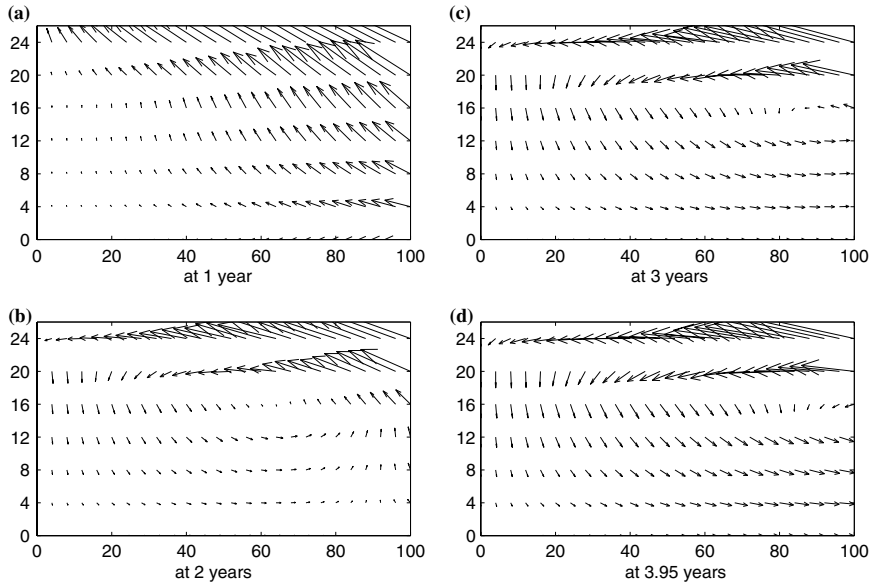

Figure 6. Development of a recirculating flow cell in case A, in the region [0, 200 m] × [0, 22 m].

is at quasi-hydrostatic status, leading to small advection and dispersion. As upconing proceeds, the saltwater mound becomes larger and a larger lower portion of the mound tends to be at hydrostatic regime. Once the quasi-hydrostatic regime is reached, the iso-mass-fraction (iso-mf) surfaces within this regime remains stable. The iso-mf surfaces of high mass fraction (e.g., the 0.8 iso-surface) do not move towards the well after 1 year, whereas the 0.5 iso-mf surface does not rise much, and then becomes stable after 3 years. As discussed above, the 0.2 iso-mf surface may be used to separate the lower portion of the saltwater mound from its upper portion. In the upper portion of the saltwater mound, the salt transport depends on both advection and hydrodynamic dispersion, which is affected by both longitudinal and transversal dispersivity. The advective salt transport behaves like the air current climbing to the peak of the saltwater mound essentially at hydrostatic status, and thus the advective transport depends on the time-dependent shape of the saltwater mound. As the saltwater mound rises, the transition zone widens, and the low iso-mf surfaces rise locally towards the well.

At $t = 3.95$ years, the salinity of the pumped water reaches 2%, and the well is shut off. Immediately after the well's shutoff, a large counterclockwise circulating flow is caused by gravity imbalance (Figure 8). This flow sweeps saltwater downward in the saltwater mound, which undergoes decay and tends to decay back to the pre-pumping regime (Figures 3 and 7).

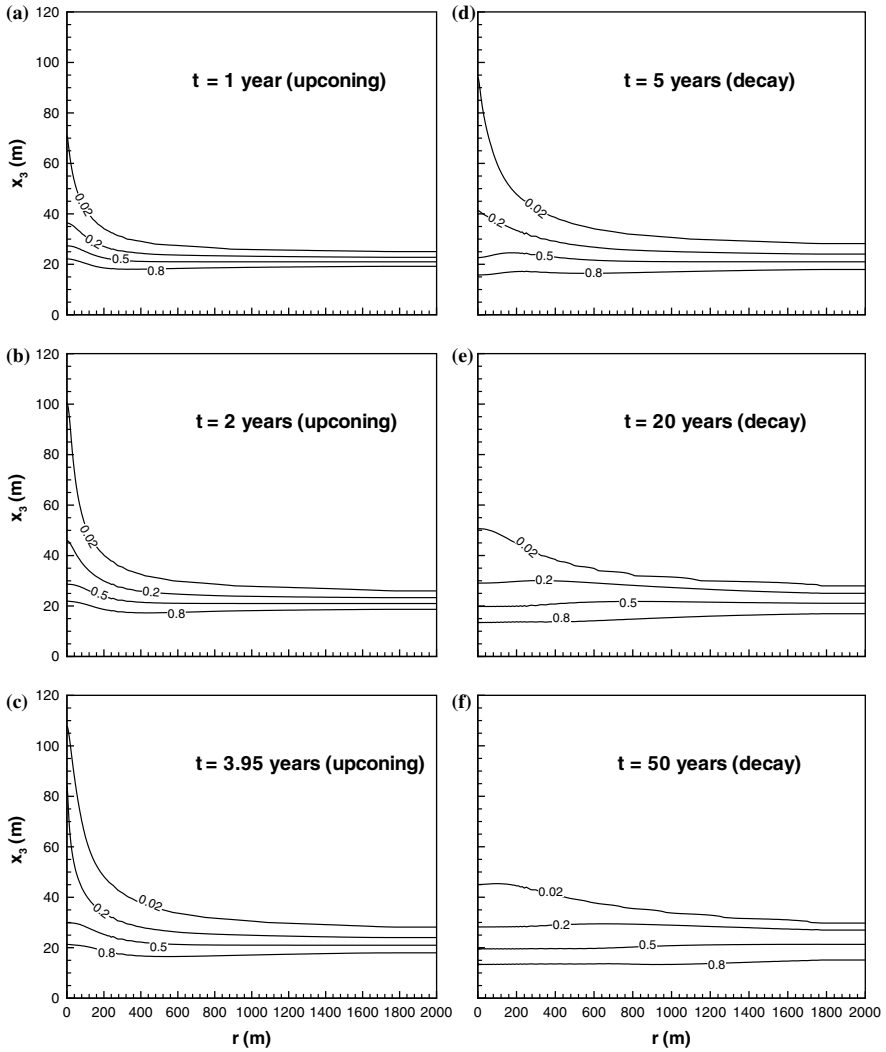

Figure 7. Transient distributions of normalized mass fraction in case A ($\alpha_L = 1.0\,\mathrm{m}$ and $\alpha_T = 0.5\,\mathrm{m}$). The left-side panel indicates results under well pumping, while the right-side one indicates results during the period of decay following the well's shut-off.

The maximum sweeping velocity occurs at the 0.1 iso-mf surface close to the inner radial boundary. As seen from Equation (7), the vertical velocity depends on both vertical gradient of reference head and the mass fraction. Above the maximum-velocity point, the mass fraction is small and not large enough to produce a large velocity, whereas under this point, the vertical gradient of reference head is large enough to tradeoff the second term of a large mass fraction in Equation (7), leading to a small vertical

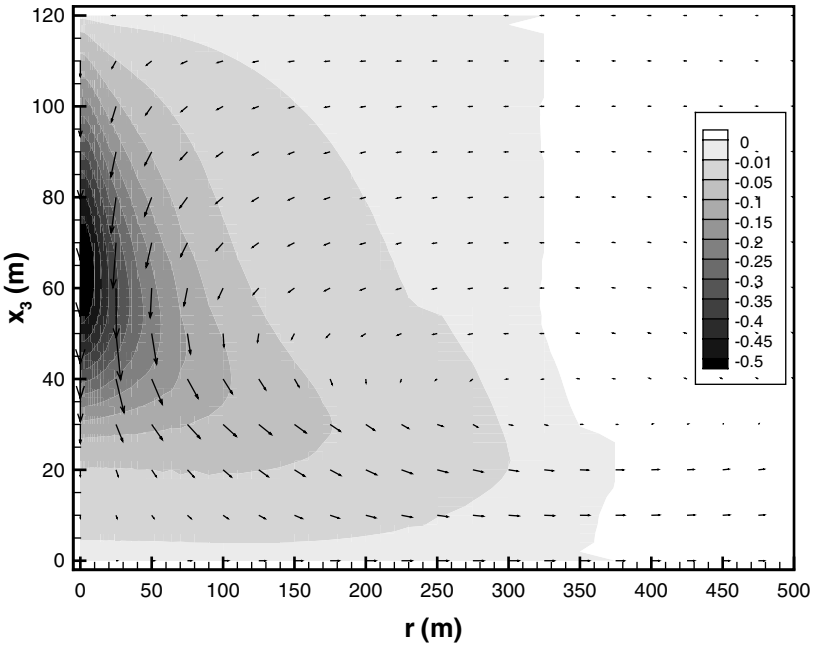

Figure 8. Contour of vertical velocity (m/d) and velocity vector field at $t = 5$ years during the period of decay following the well's shut-off in case A.

velocity too (Figure 8). As a result, the 0.1 iso-mf surface migrates back faster than the 0.02 iso-mf surface (Figure 7d). However, it takes a long time for the whole system to completely return to the initial horizontal saltwater layer. Meanwhile, the transition zone widens in the vertical direction out of the saltwater–mound region. In terms of the width of the transition zone, the system will never reverse to the initial one. This long-time decay process and irreversible features are due to the absence of regional flow. Bear *et al*. (2001) found a reversible decay process following the well's shut-off in a coastal aquifer with regional freshwater flow to the sea.

Traditionally, it is believed that the 0.5 iso-mf surface obtained by the transition zone model represents the sharp interface obtained by a sharp interface model under the same pumping condition. If this is true, we can conclude, from our simulation results, that the sharp-interface approximation overestimates the critical pumping rate or underestimate the critical rise for a given pumping rate. In the transition zone model, pumping freshwater can be maintained for a time without well salinization at a pumping rate lower than that predicted by a sharp interface model, mainly because of the involved hydrodynamic dispersion. Reilly and Goodman (1987) compared results from both the transition zone model and a sharp interface model, and found that the 0.5 iso-mf surface obtained by

the transition zone model was much higher than the sharp interface using the maximum permissible pumping rate (for the sharp interface model), whereas they were closer to each other for a reduced rate by half. Even for the latter case (Comparison 2, Reilly and Goodman, 1987), the steady-state mass fraction of the pumped water was as high as 4.2%, indicating the pumped water may not be used for drinking water.

4.3. EFFECT OF DISPERSIVITY

To demonstrate the effect of longitudinal and (mainly) transversal dispersivities on the coupled flow and salt transport, we simulate the entire transient processes of upconing and decay within 50 years for cases B and C with $\beta_C = 0.025$. The very small transversal dispersivity in case B is used to demonstrate whether the FEAS code can produce a narrow transition zone with small or no numerical dispersion. Because different flow and transport regimes are obtained in the same simulation time for different values of dispersivities (cases A, B, and C), we compare the transport regimes among the three cases at the simulation time just before well's shut-off (when the pumped water contains 2% saltwater) and at 50 years.

Figure 9 presents the normalized mass-fraction distributions in cases B and C when the well is shut-off, and at 50 years. In cases A, B, and C, the well is shut-off at 3.95, 11.35, and 2.55 years, respectively. This indicates that the transversal (and longitudinal) dispersivity has a significant effect on the duration of well pumping for freshwater utilization. The smaller the dispersivities are, the longer the well pumps freshwater. For example, the pumping duration in case B is about three times that of case A, while the transversal dispersivity in case B is 25 times smaller than that in case A. Figure 10a shows the breakthrough curves of the normalized mass fraction in pumped water for the three cases. We can see that in case B, the breakthrough curve exhibits the slowing-down of the rate of increase (with respect to time) in the mass-fraction of the pumped water. The conclusion on the pumping duration implies that the well can pump freshwater longer in a rather homogeneous aquifer than in a highly heterogeneous aquifer, because of the macrodispersivity (Dagan, 1989; Gelhar, 1993), when both aquifers have the same flow and transport properties (e.g., α_L and α_T).

The transition zone is different in the three cases in terms of (a) its width in the far region, and (b) the saltwater mound shape in the upconing region. The transition zone is very narrow in case B because of the small transversal dispersivity used. In the far region, the flow is essentially horizontal, and the width of the transition zone is dominated by the transversal dispersivity. In case C, the largest transversal dispersivity used produces the widest transition zone at the time of well's shut-off. The wide transition

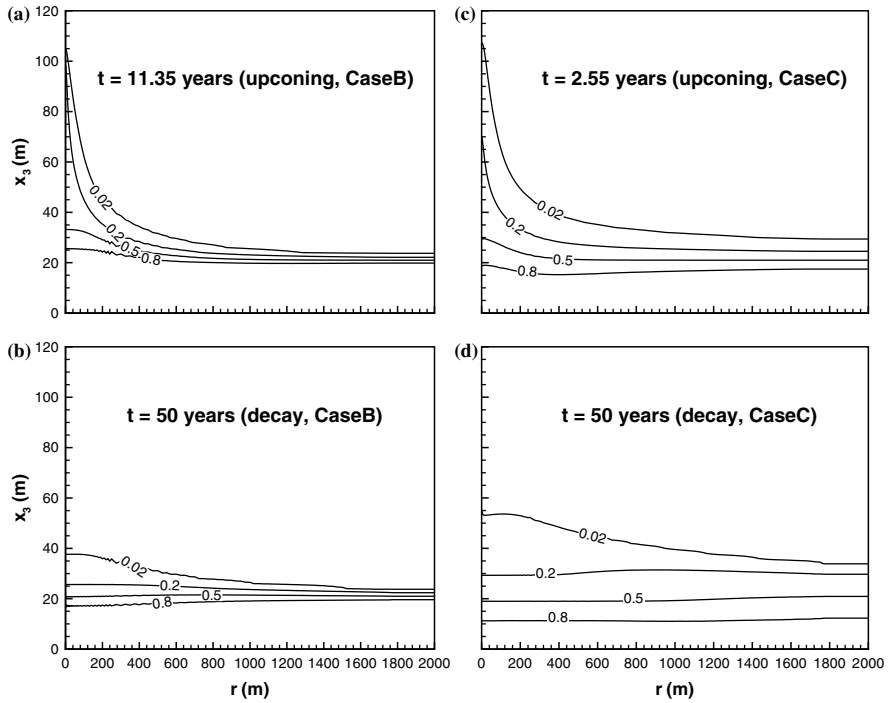

Figure 9. The normalized mass fraction distributions at (a) 11.35 years, (b) 50 years in case B ($\alpha_L = 0.2$ m and $\alpha_T = 0.02$ m), (c) 2.55 years, and (d) 50 years in case C ($\alpha_L = 10$ m and $\alpha_T = 1.0$ m).

zone can shorten the pumping duration because of the shorter distance for salt particles to arrive at the well. Regarding the shape of the saltwater mound, we can see (from the shape of 0.02 iso-mf surface) that the entire mound in the horizontal cross-section is narrower in case B than in case C. The smaller radius of the saltwater mound in the cross-section produces higher mass fraction in the center of the mound. For example, the 0.2 iso-mf surface reaches the well in case B, while it reaches at $x_3 = 72$ m in case C. This is understandable in that the total salt flux discharged by the well should be identical at the well's shut-off for different cases (say, 2% of normalized mass fraction in pumped water). A narrow cross-section of mixed water will require a higher mass fraction along the cross section. At $t = 50$ years, after a long time decay process, different transition zones are obtained for different cases (see Figures 7 and 9). The decay, or recovery, process takes a shorter time in case B than in case C. The narrow transition zone remains unchanged in case B, while the transition zone at $t = 50$ years becomes wider in both cases A and C than that at the time of the well's shut-off. For all the three cases, the decay process is slow and requires a very long time to completely recover. In summary, an increase in

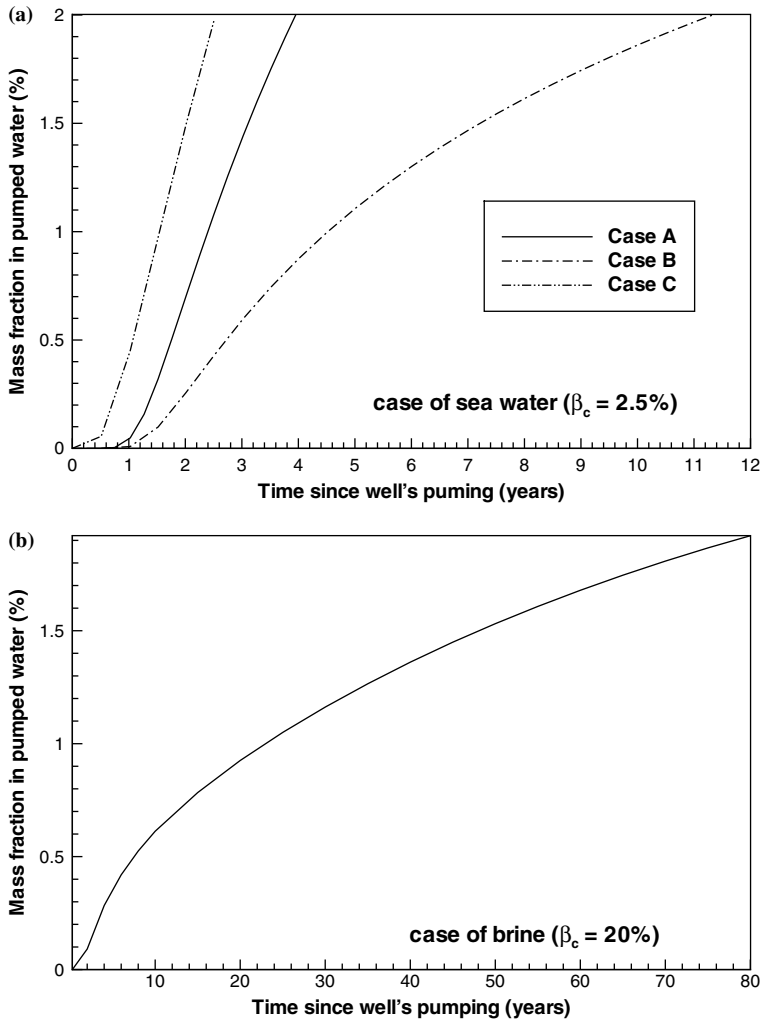

Figure 10. Breakthrough curves of the normalized mass fraction in the pumped water in the case of (a) seawater ($\beta_c = 0.025$) and (b) brine ($\beta_c = 0.20$).

dispersivity, especially the transversal one, leads to a wider transition zone, a flatter salinity mound, an earlier well shut-off, and a longer decay period of the upconed saltwater mound.

The obtained narrow transition zone in case B demonstrates that the FEAS code can be used to simulate transport with small or no numerical dispersion. The reason for this advantage of the code is that the advective–dispersive transport equation is solved in the Eulerian–Lagrangian framework in two steps: (1) the Lagrangian mass fraction is derived by the adaptive pathline-based particle tracking algorithm (Bensabat *et al.*, 2000), and

(2) the remaining dispersion equation is then solved by the Galerkin FEM. The particle tracking algorithm used can accurately track particles within a complicated flow field by adaptively cutting the simulation time step size into a number of tracking time steps. This code does not suffer from the instability constraint of the Peclet number in the advection-dominated transport in the vicinity of the well.

4.4. EFFECT OF DENSITY DIFFERENCE FACTOR, β_C

To investigate the effect of a density difference between the freshwater and the saltwater (seawater or brine) on the upconing and decay processes, we analyze sensitivity of β_C by running three cases with different β_C values ($\beta_C = 0.0$, 0.025, 0.2). The dispersivities used are $\alpha_L = 1.0$ m and $\alpha_T = 0.5$ m. We compare the normalized mass fraction distributions in the three cases at the simulation time of well's shut-off (see Figures 11 and 7c). In the case of $\beta_C = 0.0$ (representing an ideal tracer), the transient solute mass-fraction distributions do not affect the fluid's flow, leading to the uncoupled flow and transport. The pumping duration is 452 days, much less than 3.95 years in the case of $\beta_C = 0.025$, indicating that the density effect can help retard the solute transport toward the well. Unlike in the case of $\beta_C = 0.025$, the iso-mf surfaces of both low and high mass fractions upcone towards the pumping well, resulting in the earlier shut-off of the well. Although the dispersivities used in both cases are the same, the transition zone at the time of well's shut-off behaves differently: the transition zone is narrower in the $\beta_C = 0.0$ case than the $\beta_C = 0.025$ case. However, the transition zone in Figure 11a ($t = 452$ days) is close to that in Figure 7a ($t = 1$ year), indicating that the transition zone away from the solute mound depends primarily on the transversal dispersivities because the flow is essentially horizontal.

The most interesting comparison of the normalized mass fraction distributions is between the cases of $\beta_c = 0.025$ (seawater) and $\beta_c = 0.20$ (brine) (Figures 7c and 11b). In the latter case, the well can pump freshwater (in terms of 2% mass fraction of brine, rather than absolute salt mass fraction) for 80 years until the normalized mass fraction of the pumped water increases up to 2%. The saltwater mound is composed of only low mass fraction fluid ($C < 0.2$), while the iso-mf surfaces of high mass fraction ($C > 0.2$) are almost horizontal straight lines (= horizontal surfaces), indicating that the salt mass migrating toward the well comes from the upper portion (with smaller mass fraction) of the transition zone. This indicates that the heavier brine in the lower portion tends to stay there (practically) without responding to the pumping. The transition zone is much wider and the saltwater mound is also much wider in terms of its radius. Therefore, the density difference factor plays a key role in the coupled density-dependent

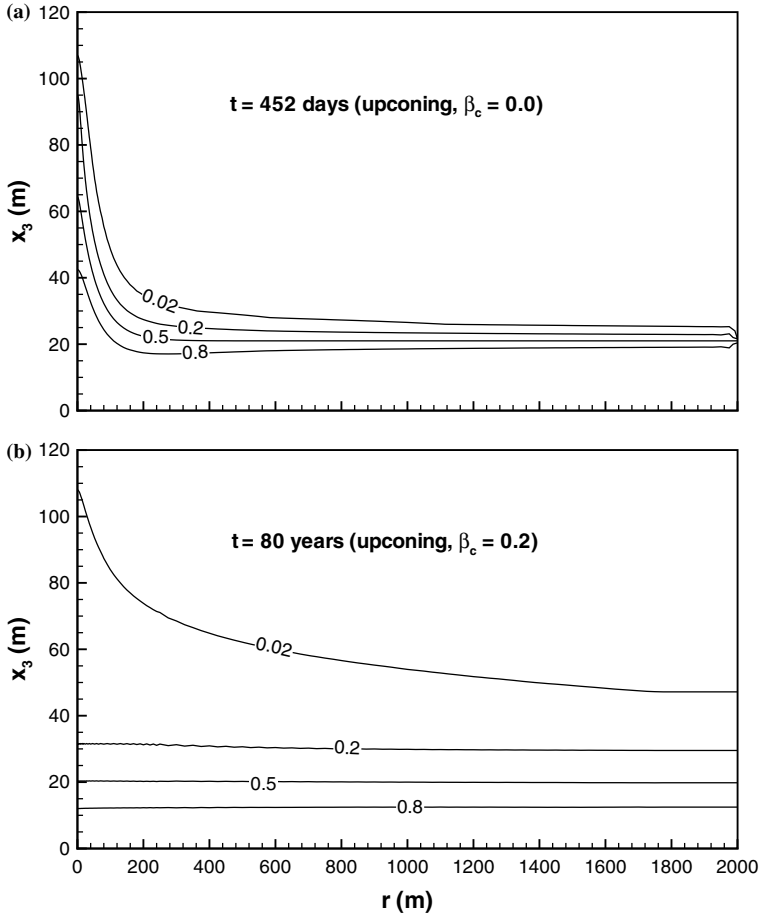

Figure 11. The normalized mass fraction distributions of (a) a tracer ($\beta_c = 0.0$) at 452 days of pumping, and (b) brine ($\beta_c = 0.20$) at 80 years of pumping in the case of $\alpha_L = 1.0$ m and $\alpha_T = 0.5$ m.

flow and transport and the difference between the weakly (seawater) and strongly coupled (brine) flow and transport is significant.

These findings of the effects of density difference factor are similar to those obtained in a series of laboratory experiments conducted in a three-dimensional cubical domain, referred to as "saltpool", by Oswald (1998), Oswald *et al.* (2002), and Johannsen *et al.* (2002). In their phase 3 experiments (Johannsen *et al.*, 2002, Figure 1), the saltwater initially takes the form of a horizontal layer below the freshwater in the cube. Freshwater was then injected into the system through an upper inflow hole, and mixed water was displaced out of this system through an upper discharge hole located at the diagonal line with the inflow hole. The entire transient

saltwater distribution was recorded as a benchmark problem for density-dependent flow and transport. Two saltwater solutions with different salt-mass fractions ($\omega = 0.01,\ 0.10$) were used. Johannsen *et al.* (2002) numerically reproduced the saltwater upconing problem conducted in the laboratory experiments for the two selected salt solutions. In the case of $\omega = 0.10$, the iso-mf surfaces of high normalized mass fractions (e.g., 0.5 and 0.9) lie horizontally in the transition zone, while only the mixed water with lower mass fractions was discharged out of the system (Oswald *et al.*, 2002; Johannsen *et al.*, 2002, Figure 6).

For water supply, the water quality in the pumped water may be based on the absolute mass-fraction of salt, which is independent of salt mass-fraction of the saltwater. For this purpose, we can also compare the simulation results for the seawater ($\beta_C = 0.025$) and brine ($\beta_C = 0.20$). From the breakthrough curve of normalized mass-fraction in the pumped water shown in Figure 10b, we can see the shut-off time is at $t = 3.9$ years, at which the pumped water contains 0.25% mass-fraction of brine, having the same absolute salt mass-fraction as 2% mass-fraction of seawater. The duration of pumping essentially freshwater is close in both cases. However, the mass-fraction contours at the well's shut-off time in both cases are different. In the brine case, the saltwater mound has a larger radius for the same absolute salt mass-fraction as in the seawater case. The brine zone of high normalized mass-fraction is always at hydrostatic status because of a higher density effect. The salt transport happens in the upper layer of very low normalized mass-fraction in the transition zone due to hydrodynamic dispersion. Unlike the upconing beneath the pumping well in the seawater case, smaller advective transport of salt occurs beneath the well in the brine cases, and more salt has to be transported from far region away from the well vicinity.

5. Conclusions

In many aquifers, the upconing of saltwater underlying the freshwater zone can cause the contamination/salinization of pumped freshwater. The salinity of the pumped water and the period of pumping essentially freshwater depend, among others, mainly on the density difference factor and the dispersivity of the aquifers. The process of decay of the upconed saltwater mound, following the shut-off of the salinized well, is critical to restoring salinized aquifers and reusing the freshwater in the restored aquifers.

The mathematical model for strongly density-dependent flow and salt transport, implemented in the FEAS code, was presented. The numerical modeling techniques in the code were briefly described and the Eulerian–Lagrangian framework and the adaptive pathline-based particle–tracking algorithm for solving the advective–dispersive salt transport

equation were addressed. The code was used to simulate the transient processes of the upconing and saltwater–mound decay following the well's shut-off in an axially symmetrical system, with different density difference factor (for an ideal tracer, seawater, and brine) and dispersivities. For each case, the pumping process and saltwater upconing were continued until the normalized mass fraction of the pumped water reached a certain criterion (2%). The simulation results for seawater of moderate value of density difference factor show that as the pumping proceeds, the saltwater mound becomes larger in the vertical direction and wider in the horizontal direction. The saltwater mound may consist of two separate subregions: salt transports to the pumping well by both advection and dispersion in the upper subregion for iso-mf surfaces of low normalized mass fractions, while the lower subregion with high mass fractions is at quasi-hydrostatic status with negligible advection and dispersion and practically does not shift much toward the pumping well. Following the salinized well's shut-off, the upconed saltwater mound undergoes decay and tends to decay back to the pre-pumping regime under the large counterclockwise circulating flow caused by gravity imbalance. However, in terms of the width of the transition zone, the system will never reverse to the initial one, leading to an irreversible decay process because of the absence of regional flow.

It was found that the upconing–decay process is sensitive to both transversal dispersivity and longitudinal dispersivity. Smaller values of dispersivities produce longer period of pumping freshwater, and shorter time for the decay process. The study case of small dispersivity values produces a very narrow transition one, indicating that the FEAS code can be used for transport simulation with small or no numerical dispersion. This may be attributed to the Eulerian–Lagrangian framework used for solving the advective–dispersive salt transport and adaptive pathline-based particle-tracking algorithm used. This code does not suffer from the instability constraint of Péclet number.

Comparison among the three cases with different density difference factor values revealed that the density effect retards the solute transport toward the pumping well and prolongs the pumping duration prior to salinization. For brine with a high density difference factor of 0.2, the saltwater mound contains mixed water of very small normalized mass fraction, while all other mixed water lie horizontally in the lower portion of the transition zone. The findings on local upconing of brine are consistent with those obtained in laboratory experiments conducted in a three-dimensional cubical domain (Johannsen *et al.*, 2002; Oswald *et al.*, 2002). The findings for brine may imply that the traditional sharp interface model cannot produce a reasonable approximation for brine transport, because the 0.5 iso-mass-fraction surface of brine remains (practically) horizontal, rather than upconing toward the well.

References

Axelsson, O. and Barker, V. A.: 1984, *Finite Element Solution of Boundary Value Problem, Theory and Computation*, Academic Press, Orlando.

Ajiz, M. A. and Jennings, A.: 1984, A robust incomplete Choleski conjugate gradient algorithm, *Int. J. Numer. Methods Eng.* **20**, 949–966.

Barrett, R., Berry, M., Chan, T. F., Demmel, J., Donato, J. M., Dongarra, J., Eijkhout, V., Pozo, R., Romine, C. and Van der Vorst, H.: 1994, *Templates for the Solution of Linear Systems: Building Blocks for Iterative Methods*, SIAM, Philadelphia.

Bear, J. and Dagan, G.: 1964, Moving interface in coastal aquifers, *Proc. ASCE 99(HY4)*, 193–216.

Bear, J.: 1979, *Hydraulics of Groundwater*, McGraw-Hill, New York.

Bear, J. and Verruijt, A.: 1990, *Modeling Groundwater Flow and Pollution*, Kluwer Academic Publishers, Dordrecht.

Bear, J. and Bachmat, Y.: 1991, *Introduction to Modeling of Transport Phenomena in Porous Media*, Kluwer Academic Publishers, Dordrecht.

Bear, J., Cheng, A. H-D., Sorek, S., Ouazar, D. and Herrera I. (eds.): 1999, *Seawater Intrusion in Coastal Aquifers – Concepts, Methods and Practices*, Kluwer Academic Publishers, Dordrecht.

Bear, J., Zhou, Q. and Bensabat, J.: 2001, Three dimensional simulation of seawater intrusion in heterogeneous aquifers: application to the coastal aquifer of Israel, in: *proceedings of the First International Conference on Saltwater Intrusion and Coastal Aquifers-Monitoring, Modeling, and Management*, Essaouira, Morocco, April 23–25.

Bennett, G. D., Mundorff, M. J. and Hussain, S. A.: 1968, *Electric-Analog Studies of Brine Coning Beneath Freshwater Wells in the Punjab Region*, West Pakistan, U.S. Geological Survey Water-Supply Paper, 1608-J.

Bensabat, J., Zhou, Q. and Bear, J.: 2000, An adaptive pathline-based particle tracking algorithm for the Eulerian-Lagrangian method, *Adv. Water Resour.* **23**(4), 383–397.

Bower, J. W., Motz, L. H. and Durden, D. W.: 1999, Analytical solution for determining the critical condition of saltwater upconing in a leaking artesian aquifer, *J. Hydrol.* **221**, 43–54.

Dagan, G., 1989, *Flow and Transport in Porous Formations*, Springer-Verlag, Berlin.

Dagan, G. and Zeitoun, D. G.: 1998, Free-surface flow toward a well and interface upconing in stratified aquifers of random conductivity, *Water Resour. Res.* **34**(11), 3191–3196.

Diersch, H. J., Prochnow, D. and Thiele, M.: 1984, Finite element analysis of dispersion-affected saltwater upconing below a pumping well, *Appl. Math. Model* **8**(5), 305–312.

Gelhar, L. W.: 1993, *Stochastic Subsurface Hydrology*, Prentice Hall, Englewood Cliffs.

Haitjema, H. M.:1991, An analytic element model for transient axi-symmetric interface flow, *J. Hydrol*. **129**, 215–244.

Hassanizadeh, S. M. and Leijnse, A.: 1988, On the modeling of brine transport in porous media, *Water Resour. Res.* **24**, 321–330.

Haubold, R. G.: 1975, Approximation for steady interface beneath a well pumping freshwater overlying saltwater, *Ground Water* **13**(3), 254–259.

Herbert, A. W., Jackson, L. P. and Lever, D. A.: 1988, Coupled groundwater flow and solute transport with fluid density strongly dependent upon concentration, *Water Resour. Res.* **24**, 1781–1795.

Kemblowski, M.: 1987, The impact of the Dupuit–Forchheimer approximation on saltwater intrusion simulation, *Ground Water* **25**(3), 331–336.

Johannsen K., Kinzelbach, W., Oswald, S. and Wittum G.: 2002, The saltpool benchmark problem – numerical simulation of saltwater upconing in a porous medium, *Adv. Water Resour.* **25**, 335–348.

Lever, D. A. and Jackson, C. P.: 1985, On the equations for the flow of a concentrated salt solution through a porous medium, Harwell Rep. AERE-R. 11765, HMSO, London.

Ma, T-S., Sophocleous, M., Yu, Y-S. and Buddemeier, R. W.: 1997, Modeling saltwater upconing in a freshwater aquifer in south–central Kansas, *J. Hydrol.* **201**, 120–137.

Muskat, M. and Wyckoff, R. D.: 1935, An approximate theory of water-coning in oil production, *Trans. Am. Inst. Min. Metall. Petrol. Eng.* **114**, 144–163.

Muskat, M.: 1937, *The Flow of Homogeneous Fluids Through Porous Media*, McGraw-Hill, New York.

Neuman, S. P.: 1984, Adaptive Eulerian–Lagrangian finite element method for advection-dispersion, *Int. J. Numer. Methods Eng.* **20**, 321–337.

Oswald, S. E.: 1998, Density-driven flow in porous media: three-dimensional experiments and modeling, PhD Thesis, Institute of Hydromechanics and Water Resources Management, ETH Zurich, Switzerland.

Oswald, S. E., Scheidegger, M. B. and Kinzelbach, W.: 2002, Time-dependent measurement of strongly density-dependent flow in a porous medium via nuclear magnetic resonance imaging, *Transport Porous Media* **47**(2), 169–193.

Pinder, G. F., and Page, R. H.: 1977, Finite element simulation of salt water intrusion on the South Fork of Long Island, In: *Finite Elements in Water Resources*, *Proceeding of the 1st international Conference Finite Elements in Water Resources*, Pentech, London, pp. 2.51–2.69.

Reilly, T. E. and Goodman, A. S.: 1987, Analysis of saltwater upconing beneath a pumping well, *J. Hydrol.* **89**, 169–204.

Reilly, T. E., Frimpter, M. H., LeBlanc, D. R. and Goodman, A. S.: 1987, Analysis of steady-state salt-water upconing with application at Truro well field, Cape Code, Massachusetts, *Ground Water* **25**(2), 194–206.

Rubin, H. and Pinder, G. F.: 1977, Approximate analysis of upconing, *Adv. Water Resour.* **1**(2), 97–101.

Sahni, B. M.: 1973, Physics of brine upconing beneath skimming wells, *Ground Water* **11**(1), 19–24.

Strack, O. D. L.: 1972, Some cases of interface flow towards drains, *J. Eng. Math.* **6**, 175–191.

Voss, G. I. and Souza, W. R.: 1987, Variable density flow and solute transport simulation of regional aquifers containing a narrow freshwater-saltwater transport zone, *Water Resour. Res.* **23**(10), 1851–1866.

Weast, R. C. (ed.): 1989, *Handbook of Chemistry and Physics*, 70th edn, Chemical Rubber Publishing Company (CRC), Boca Raton, Florida.

Wirojanagud, P. and Charbeneau, R. J.: 1985, Saltwater upconing in unconfined aquifers, *J. Hydraul. Eng.*, ASCE **111**(3), 417–434.

Zhou, Q.: 1999, *Modeling seawater intrusion in coastal aquifers*, PhD Thesis, Technion-Israel Institute of Technology.

Zhou, Q., Bensabat, J. and Bear, J.: 2001, Accurate calculation of specific discharge in heterogeneous porous media, *Water Resour. Res.* **37**(12), 3057–3069.